
LATENT WATERMARK: INJECT AND DETECT WATERMARKS IN LATENT DIFFUSION SPACE

Zheling Meng

Center for Research on
Intelligent Perception and Computing,
State Key Laboratory of
Multimodal Artificial Intelligence Systems,
Institute of Automation,
Chinese Academy of Sciences
zheling.meng@cripac.ia.ac.cn

Bo Peng

Center for Research on
Intelligent Perception and Computing,
State Key Laboratory of
Multimodal Artificial Intelligence Systems,
Institute of Automation,
Chinese Academy of Sciences
bo.peng@nlpr.ia.ac.cn

Jing Dong*

Center for Research on
Intelligent Perception and Computing,
State Key Laboratory of
Multimodal Artificial Intelligence Systems,
Institute of Automation,
Chinese Academy of Sciences
jdong@nlpr.ia.ac.cn

ABSTRACT

Watermarking is a tool for actively identifying and attributing the images generated by latent diffusion models. Existing methods face the dilemma of image quality and watermark robustness. Watermarks with superior image quality usually have inferior robustness against attacks such as blurring and JPEG compression, while watermarks with superior robustness usually significantly damage image quality. This dilemma stems from the traditional paradigm where watermarks are injected and detected in pixel space, relying on pixel perturbation for watermark detection and resilience against attacks. In this paper, we highlight that an effective solution to the problem is to both inject and detect watermarks in the latent diffusion space, and propose Latent Watermark with a progressive training strategy. It weakens the direct connection between quality and robustness and thus alleviates their contradiction. We conduct evaluations on two datasets and against 10 watermark attacks. Six metrics measure the image quality and watermark robustness. Results show that compared to the recently proposed methods such as StableSignature, StegaStamp, RoSteALS, LaWa, TreeRing, and DiffuseTrace, LW not only surpasses them in terms of robustness but also offers superior image quality. Our code will be available at <https://github.com/RichardSunnyMeng/LatentWatermark>.

Keywords Latent diffusion model, Watermark, Latent space

1 Introduction

Recently, latent diffusion models Nichol et al. [2022], Rombach et al. [2022], Gu et al. [2022] are developing rapidly and have made many important breakthroughs in high-fidelity image generation. Trained on a large-scale dataset, a latent diffusion model can generate images with high resolution and quality according to text descriptions Rombach et al. [2022]. By efficient and effective fine-tuning Hu et al. [2021], some methods can generate images on specific scenarios and subjects. Besides open-source models, many online platforms also provide similar services to the public. While bringing convenience to our daily lives and work, they inevitably bring information security risks to our society.

*Corresponding Author

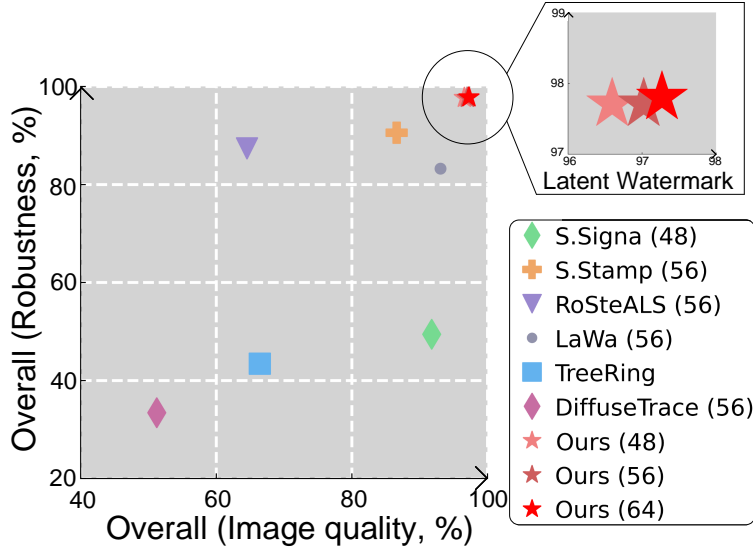


Figure 1: The overall performance of image quality and watermark robustness on the MS-COCO 2017 evaluation Lin et al. [2014] for StableSignature (S.Signa., 48 bits) Fernandez et al. [2023], StegaStamp (S.Stamp, 56 bits) Tancik et al. [2020], RoSteALS (56 bits) Bui et al. [2023], LaWa (48 bits) Rezaei et al. [2024], TreeRing Wen et al. [2023], DiffuseTrace (56 bits) Lei et al. [2024], as well as our proposed Latent Watermark (48 bits, 56 bits, and 64 bits). Please see Sec.4.1 for more details about the overall performance calculation.

For example, some individuals use diffusion models to fabricate fake news, creating social panic and disrupting social order Barrett et al. [2023]. And some people create and spread rumors to defame the reputation of others. Methods that can identify images generated by latent diffusion models and determine their sources are urgently needed.

There are two main routes for identifying generated images, i.e. passive identification and active identification Raja [2021]. Passive identification methods learn and extract forgery traces left by generators in spatial or frequency domain Wang et al. [2020], Qian et al. [2020], Chai et al. [2020]. However, they usually cannot accurately identify generators unseen in training sets Corvi et al. [2023], Lorenz et al. [2023], Ricker et al. [2023]. Besides, they cannot attribute users who access the services to generate images. In contrast, active identification injects an invisible watermark into generated images before releasing them Fernandez et al. [2022], Tancik et al. [2020], Xiong et al. [2023], Nguyen et al. [2023], Bui et al. [2023], Fernandez et al. [2023], Zhao et al. [2023a], Wen et al. [2023]. The watermarks, usually in the form of multi-bit messages, can help to identify generated images (identification task) and attribute their sources (attribution task) He et al. [2020], Zhong et al. [2020], Fang et al. [2022], Qin et al. [2024], Li et al. [2024]. The watermarking methods for latent diffusion models are attracting more and more attention.

Existing watermarking methods for latent diffusion models can be classified into three categories, i.e. executing watermark algorithms before Fernandez et al. [2023], during Nguyen et al. [2023], Wen et al. [2023], and after generating images Tancik et al. [2020], Bui et al. [2023]. A good watermarking method should satisfy strong robustness and high image quality. Strong robustness helps resist attacks from intentional and unintentional damages. High image quality can alleviate the concerns among model developers regarding its potential negative impact on their generative models, thereby encouraging the widespread application of the method. The injection of watermarks should be done in an imperceptible manner and should not change or even limit the generation ability of vanilla models. However, existing methods often exhibit a trade-off between image quality and watermark robustness. We evaluate four previous methods that have been reported to have good performance, i.e. StegaStamp Tancik et al. [2020], StableSignature Fernandez et al. [2023], RoSteALS Bui et al. [2023], and LaWa Rezaei et al. [2024]. We show their overall performance of image quality and watermark robustness in Fig.1. Please refer to Sec.4.1 for more details about the results. It can be seen that StegaStamp and RoSteALS have better robustness but worse image quality, while StableSignature and LaWa has better quality but worse robustness.

We highlight that the dilemma stems from **the watermarking paradigm** where watermarks are injected and detected in pixel space, which is used by most of existing methods Fernandez et al. [2022], Tancik et al. [2020], Xiong et al. [2023], Nguyen et al. [2023], Bui et al. [2023], Fernandez et al. [2023], Zhao et al. [2023a]. The paradigm guides watermarking

models to inject watermarks in a manner of pixel perturbation. When the magnitude of this perturbation is small, it is not enough to resist various attacks. When the magnitude is large, image quality is severely affected.

In this paper, we propose **Latent Watermark (LW)** to watermark and detect images generated by latent diffusion models in latent space. Our motivation is that if watermarks are injected and detected in latent diffusion space, we can **avoid directly relying on pixel perturbation** for watermark detection and resilience against attacks. It weakens the correlation between image quality and watermark robustness with the latent encoder and decoder.

However, our experiments reveal that injecting and detecting watermarks using LW with a high image quality and robustness is not easy. Our method inserts four modules for watermark injection and detection. The challenge mainly lies in training these modules. The analysis in Sec.4.4.1 reveals that it is necessary to involve the latent encoder and decoder in the training to improve image quality and robustness. In the training phase, the latent images with watermarks are first decoded into the pixel images by the latent decoder, and then encoded into the latent images by the latent encoder for watermark detection. When employing random initialization for parameters, the initial parameters of these modules are distant from their globally optimal solutions. This discrepancy hinders the effective adaptation between the input/output of each module and the frozen latent encoder/decoder, leading the training process to converge towards local solutions. To address this challenge, in the manuscript, we propose a three-step progressive training strategy, which trains the watermark modules from local to global while freezing the weights of the vanilla model. The motivation stems from the idea of divide-and-conquer: first pre-train each module separately and then fine-tune them together. It provides initial points close to optimal solutions, serving as a more suitable starting point for formal training. It significantly reduces the difficulty of training and improves the training efficiency.

Some recent and concurrent studies also consider watermarking using the latent space. RoSteALS Bui et al. [2023] and LaWa Rezaei et al. [2024] inject watermarks in the latent space but detect watermarks on the pixel images directly. It makes the watermarks still rely on pixel perturbation, leading to the difficulty in balancing robustness and image quality. TreeRing Wen et al. [2023] and DiffuseTrace Lei et al. [2024] write watermarks into the initial noises sampled in the latent space. They detect watermarks by restoring the initial noises through the forward diffusion process. However, the errors between the vanilla images and the attacked images accumulate during the diffusion process, resulting in low watermark robustness. Different from them, with the help of the proposed training strategy, our method injects and detects watermarks completely in the latent space and avoids the low robustness caused by the error accumulation. Compared with these methods, it shows higher performance as presented in Fig.1.

We evaluate the performance of our methods and the previous six methods using the captions collected from MS-COCO 2017 Lin et al. [2014] and Flickr30k Young et al. [2014] datasets. Six metrics are measured in the experiments, including FID, SSIM, NIQE, and PIQE for evaluating image quality, and BitACC and TPR@0.01FPR for evaluating watermark robustness under 10 attacks. The attacks cover the destructive, constructive, and reconstructive attacks. The results illustrate that our method has better robustness and image quality compared to other methods, significantly alleviating the trade-off between them as shown in Fig.1. We also study the effectiveness of each training step, the position for watermark injection, and the size of training data on the performance of LW. Extensive discussions are also conducted.

In summary, the contributions of this paper are as follows.

- Previous methods resort to perturbations in the pixel space for watermark injection, which have difficulty in resisting attacks while maintaining image quality. Several methods attempt to use the latent diffusion space, but they either continue to rely on pixel perturbations or struggle with inferior robustness.
- We highlight injecting and detecting watermarks completely in latent diffusion space by inserting several tiny modules and propose Latent Watermark (LW). Further, we propose a progressive training strategy to address the challenge of effectively training them.
- We conduct evaluations using the captions from MS-COCO and Flickr30k datasets. 10 attacks from three categories are applied to the watermarked images. Based on six metrics, the results demonstrate that LW can inject more robust watermarks with higher image quality.

2 Related Work

2.1 Latent Diffusion Model

Diffusion probabilistic models Sohl-Dickstein et al. [2015], Ho et al. [2020] are proposed to learn a data distribution $p(\tilde{x})$ from a real distribution $q(x)$ by the Markov forward and backward diffusion process. Specifically, they train a noise predictor $\epsilon_\theta(\tilde{x}_t, t)$ to generate an image \tilde{x}_0 from a sampled Gaussian noise \tilde{x}_T by estimating the noises and performing denoising for T steps. In order to speed up the generation process, Song et al. propose Denoising Diffusion Implicit Model (DDIM) Song et al. [2020] to reduce the standard 1000-step denoising process to fewer, usually 50 steps.

To reduce computational resource requirements while retaining the quality, Latent Diffusion Model (LDM) Rombach et al. [2022] performs the diffusion process in a latent space and becomes a standard paradigm for image generation using diffusion models Nichol et al. [2022], Rombach et al. [2022], Gu et al. [2022]. LDM performs denoising in the latent space with lower resolution and then uses a latent decoder $Dec(\cdot)$ to generate human-understandable images with higher resolution:

$$\begin{aligned} \tilde{x} &= Dec(\tilde{z}_0) \\ \tilde{z}_{t-1} &= \frac{1}{\sqrt{\alpha_t}} \left(\tilde{z}_t - \frac{1 - \alpha_t}{\sqrt{1 - \bar{\alpha}_t}} \epsilon_{\theta}(\tilde{z}_t, t) \right) \quad (t = 1, 2, \dots, T) \end{aligned} \quad (1)$$

where $\alpha_t = 1 - \beta_t$, $\bar{\alpha}_t = \prod_{i=1}^t \alpha_i$ and $\beta \in (0, 1)$ is a scheduled noise variance. For training the noise predictor $\epsilon_{\theta}(\tilde{z}_t, t)$ in the latent space, LDM also includes a latent encoder $Enc(\cdot)$ to encode training images. In this paper, Stable Diffusion (SD) Rombach et al. [2022], a classic model implementation for LDM, is used to introduce and evaluate our watermarking method. The shape of \tilde{z}_t and \tilde{x} is (4, 64, 64) and (3, 512, 512) respectively.

2.2 Watermarks for Latent Diffusion Models

Watermarking methods typically inject information as a series of bits within generated images in a subtly or imperceptibly manner. It allows for the determination of whether an image is generated and by which user through the detection of this injected information. For latent diffusion models, the methods can be classified into three categories according to the order of watermark algorithm execution and image generation.

Execute watermark algorithms before generation. The methods allow diffusion models to directly generate watermarked images without introducing any other modules. Zhao et al. [2023a] train unconditional or class-conditional models using watermarked training images, and generate watermarked images using a trigger prompt for text-conditional models. StableSignature Fernandez et al. [2023] roots a watermark into model weights by training a message encoder-decoder and fine-tuning the diffusion model. Once training is completed, both methods cannot change the injected messages.

Execute watermark algorithms during generation. Stable Messenger Nguyen et al. [2023] embeds an encoded bit message into latent diffusion space and decodes it from generated images. The work Xiong et al. [2023] carefully designs the fusion method for encoded messages and latent images. It also proposes a secure mechanism that can overcome watermark injection escape caused by simply commenting out the codes. As the most fundamental difference from our method, they both detect watermarks in pixel space via training another decoder. TreeRing Wen et al. [2023] directly writes messages in the spectrum of sampled noises and detects the messages by Gaussian noising and spectral transformation. However, it fails to attribute users, limiting its application scenarios. The proposed LW belongs to this category.

Execute watermark algorithms post generation. Given a generated image, the methods generate a generator-independent watermark and inject it into the image. StegaStamp Tancik et al. [2020] follows this way and adopts many augmentation methods in the training stage to enhance its robustness. Inspired by self-supervised learning, Fernandez et al. [2022] propose SSL-Watermarking to optimize an invisible watermark image-by-image and detect it by estimating vector cosine angles. RoSteALS Bui et al. [2023] encodes input images into a latent space by a well trained autoencoder and then injects encoded messages. Same as Nguyen et al. [2023] and Xiong et al. [2023], the methods also detect watermarks in pixel space via training another decoder.

2.3 Watermark Attacks

The purpose of watermark attack experiments is to evaluate the robustness of watermarking methods when faced with malicious or unintentional image corruptions in practice. The common attacks can be classified into three categories, i.e. destructive attacks, constructive attacks and reconstructive attacks Zhao et al. [2023b]. Destructive attacks include brightness distortion, contrast distortion, JPEG compression and Gaussian noising. Constructive attacks mainly include some denoising algorithms using Gaussian kernels or Block-Matching and 3D filtering (BM3D) Dabov et al. [2007]. Recently, Zhao et al. propose reconstructive attacks Zhao et al. [2023b] to erase watermarks. They use an image reconstruction model, such as a diffusion model or a variational autoencoder, to encode semantic features of an image and regenerate it. The work highlights that a simple reconstruction model can erase watermarks injected by most existing methods.

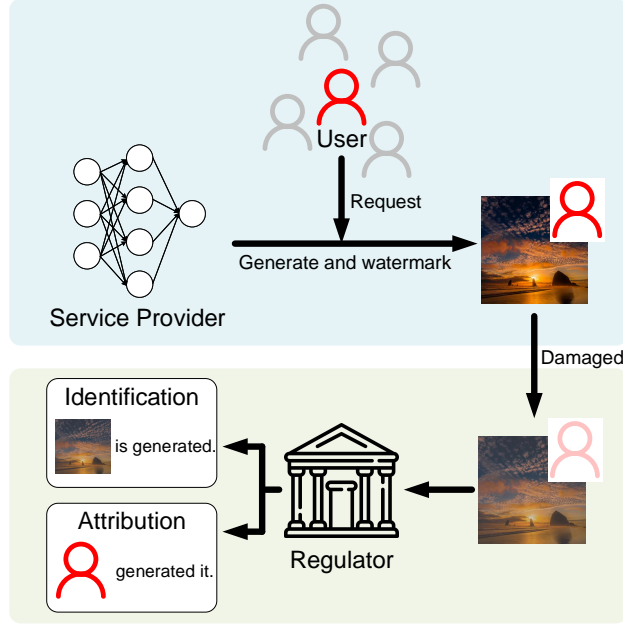


Figure 2: The threat model. The service provider generates an image according to the request of the user and watermarks it. The regulator detects the watermark of the damaged image for the identification and attribution task.

3 Methods

3.1 Threat Model

Fig.2 visualizes our threat model. There are three agents, i.e. a service provider, a user, and a regulator. Owning a latent diffusion model, the service provider provides image generation services to the public through an API. The generated images are watermarked before being released. Given a text description, the user calls the diffusion model through the API to obtain generated images. The regulator, from the service provider or government departments, completes the following two tasks by detecting watermarks:

- Identification: Determine whether an image is generated by the service provider.
- Attribution: Determine which user generates the image through the API.

The difference between the two is that the latter requires an exact match of bits. Due to unintentional and intentional damages, there are differences in image quality between generated and detected images but the contents of detected images can still be accurately understood by humans. We formally summarize the threat model as follows. We denote \tilde{x} as a generated image, distinguished from a real image x .

- Service Provider: She owns a latent diffusion model ϵ_θ and provides an API to the public to generate images watermarked by an algorithm \mathcal{T} . \mathcal{T} injects identity information in bit form into generated images while maintaining image quality so that it cannot be perceived by users.
- User: She obtains an image \tilde{x} conditioned on a text description c through the API. \tilde{x} can be changed into \tilde{x}' by common attacks as mentioned in Sec.2.3. And humans have a consistent understanding of \tilde{x} and \tilde{x}' .
- Regulator: Given \mathcal{T} , the regulator tries to identify and attribute \tilde{x}' .

3.2 Latent Watermark

Fig.3 (a) shows the structure of LW. LW is composed of a message encoder $Enc_M(\cdot)$, a message coupler $C(\cdot, \cdot)$, a message decoupler $DC(\cdot)$ and a message decoder $Dec_M(\cdot)$. Besides, a latent diffusion model, including a latent encoder $Enc(\cdot)$, a noise predictor $\epsilon_\theta(\tilde{z}_t, t)$ and a latent decoder $Dec(\cdot)$, is also needed.

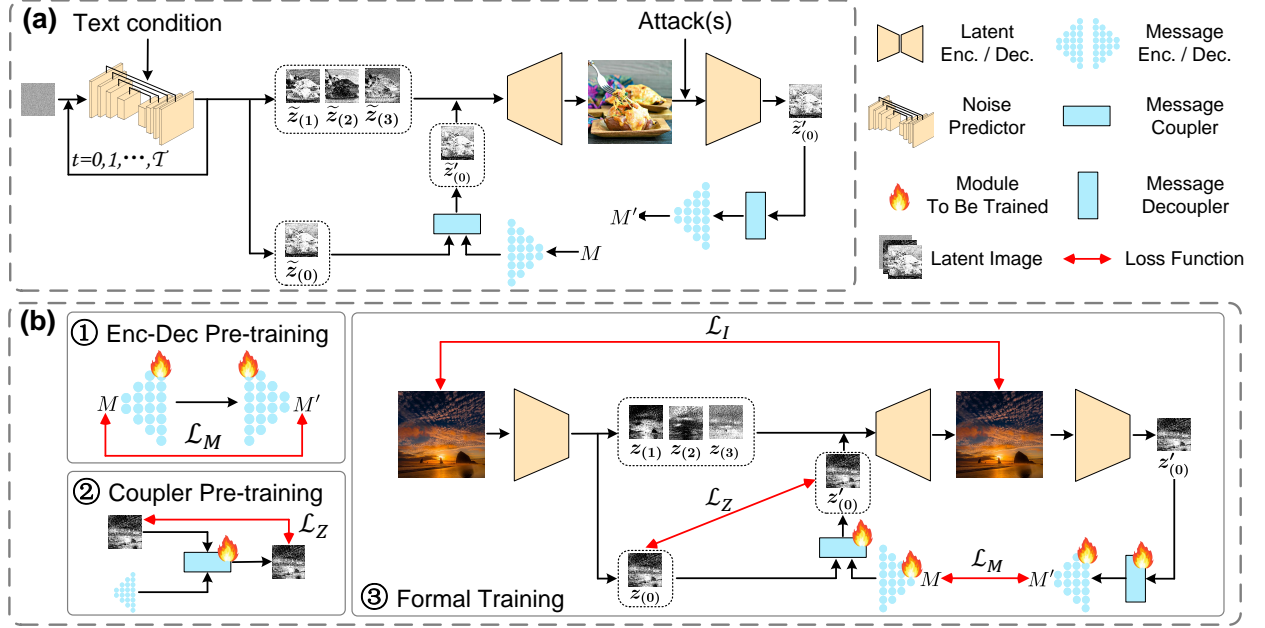


Figure 3: The proposed methods. (a) The structure of LW. (b) The three-step progressive training strategy. M : n -bit messages. $z_{(l)}$: l -th channel of latent image z .

In the stage of injecting watermarks, given a n -bit message, $Enc_M(\cdot)$ first encodes it into the latent space. Then, $C(\cdot, \cdot)$ fuses the latent image \tilde{z} from $\epsilon_\theta(\tilde{z}_t, t)$ with the encoded message to obtain \tilde{z}' . Next, \tilde{z}' is decoded by $Dec(\cdot)$ to generate an image \tilde{x} . The injecting process can be expressed as Eq.2:

$$\tilde{x} = Dec(C(\tilde{z}, Enc_M(M))) \quad (2)$$

where $M \in \{0, 1\}^n$ is a n -bit message. In the experiments, we find that choosing different channels to fuse messages will bring different performance. According to the results in Tab.3, we design $C(\cdot, \cdot)$ to fuse the first channel of \tilde{z} with the encoded messages, as shown in Fig.3 (a) and Eq.3:

$$\begin{aligned} \tilde{z}' &= C(\tilde{z}, Enc_M(M)) \\ &= C(\tilde{z}_{(0)}, Enc_M(M)) \oplus \tilde{z}_{(1)} \oplus \tilde{z}_{(2)} \oplus \tilde{z}_{(3)} \end{aligned} \quad (3)$$

where \oplus is concatenation along the channel dimension and $\tilde{z}_{(l)}$ is l -th channel of \tilde{z} ($l = \{0, 1, 2, 3\}$). $Enc_M(M)$ has the same shape with $\tilde{z}_{(l)}$.

In the stage of detecting watermarks, $Enc(\cdot)$ is used to encode an image \tilde{x}' into the latent space. Then $DC(\cdot)$ decouples the encoded message from the first channel of the latent image. Finally, $Dec_M(\cdot)$ outputs the decoding result in bit form. The detecting process can be expressed as Eq.4:

$$\begin{aligned} M' &= Dec_M(DC(\tilde{z}'_{(0)})) \\ \tilde{z}' &= Enc(\tilde{x}') \end{aligned} \quad (4)$$

where $M' \in \{0, 1\}^n$ is the decoded message.

3.3 Three-Step Progressive Training Strategy

As pointed out in Sec.1, the strategy to train LW is the key to obtain working performance. Here, we propose a progressive training strategy. Experiments in Sec.4.3 show that without it, watermark injection and image quality maintenance cannot be reached at the same time. As shown in Fig.3 (b), the training strategy includes three steps, i.e. pre-training the message encoder and decoder, pre-training the message coupler and training the model formally. For the purpose of efficiency, z from training images encoded by $Enc(\cdot)$, rather than \tilde{z} from $\epsilon_\theta(\tilde{z}_t, t)$, is used in the training stage.

Step 1: Pre-train the message encoder and decoder. In this step, the encoded messages are input into the message decoder directly to train them in the self-supervision paradigm. The loss function in this step is \mathcal{L}_1 in Eq.5:

$$\mathcal{L}_1 = \frac{1}{B \cdot n} \sum_{i=0}^{B-1} \sum_{k=0}^{n-1} (M_i^k - M_i^{k'})^2 \quad (5)$$

where $M_i \in \{0, 1\}^n$ is the i -th randomly generated message, M_i^k is k -th bit of M_i and B is the batch size. When the exponential moving average of Bit Accuracy is higher than the threshold τ_1 , the step ends.

Step 2: Pre-train the message coupler. LW is expected to inject watermarks with minimizing any impact on image quality. Therefore, optimizing the parameters of the modules should be started from the initial state, i.e., outputting the same images as the vanilla model regardless of encoded messages. In this step, the coupler will be pre-trained as an identity mapping of latent images. The loss function \mathcal{L}_2 can be expressed as Eq.6:

$$\mathcal{L}_2 = \frac{1}{|\mathcal{D}|} \frac{1}{WH} \sum_{i \in \mathcal{D}} \|z_{i(0)} - z'_{i(0)}\|_2^2 \quad (6)$$

where \mathcal{D} is the training batch with the batch size $|\mathcal{D}|$, W and H are the width and height of z_i , and z'_i is obtained using the same method outlined in Eq.3. When \mathcal{L}_2 is lower than the threshold τ_2 , the step ends.

Step 3: Train the model formally. In this step, three loss functions, i.e. \mathcal{L}_z , \mathcal{L}_I and \mathcal{L}_M , are used to train all the watermark-related modules. As shown in Eq.7, \mathcal{L}_z has the same form as Eq.6 and measures the L2 distance of latent images before and after message coupling:

$$\mathcal{L}_z = \frac{1}{|\mathcal{D}|} \frac{1}{WH} \sum_{i \in \mathcal{D}} \|z_{i(0)} - z'_{i(0)}\|_2^2. \quad (7)$$

And \mathcal{L}_I measures the visual similarity between images before and after injecting watermarks as shown in Eq.8:

$$\mathcal{L}_I = \frac{1}{|\mathcal{D}|} \sum_{i \in \mathcal{D}} LPIPS(x_i, Dec(z'_i)) \quad (8)$$

where $LPIPS(\cdot, \cdot)$ is a commonly used method for visual similarity evaluation Zhang et al. [2018]. Inspired by Nguyen et al. [2023], we supervise the message encoding and decoding by Eq.9:

$$\mathcal{L}_M = \begin{cases} \frac{1}{|\mathcal{D}| \cdot n} \sum_{i \in \mathcal{D}} \sum_{k=0}^{n-1} (M_i^k - M_i^{k'})^2 & \text{if } BitACC < \tau_3 \\ \frac{1}{|\mathcal{D}|} \sum_{i \in \mathcal{D}} \log \left(\sum_{k=0}^{n-1} \exp(M_i^k - M_i^{k'})^2 \right) & \text{otherwise} \end{cases} \quad (9)$$

where $BitACC$ represents Bit Accuracy and τ_3 is a threshold. When Bit Accuracy is high, the regression loss for bits is small and Eq.9 can help enhance the magnitude of the supervision signal. Finally, the loss function of Step 3 can be expressed by Eq.10:

$$\mathcal{L}_3 = \alpha_1 \mathcal{L}_z + \alpha_2 \mathcal{L}_I + \alpha_3 \mathcal{L}_M \quad (10)$$

where α_1 , α_2 and α_3 are the weighting coefficients. The latent diffusion model is frozen throughout the three steps.

4 Experiments, Results and Discussions

4.1 Experiment Setup

4.1.1 Datasets

Three datasets are used to train and evaluate LW. For training LW, 50,000 images are used. They are all randomly sampled from LAION-Aesthetics-5+ Schuhmann et al. [2022], which has 600M image-text pairs with predicted aesthetics scores of 5 or higher and is the training set for Stable Diffusion Rombach et al. [2022]. For evaluating LW and other methods, we randomly sample 5,000 captions from two datasets respectively, i.e. MS-COCO 2017 (COCO) Lin et al. [2014] and Flickr30k Young et al. [2014], to generate images. The captions from COCO are all sampled in the evaluation subset.

Table 1: The results on image quality and watermark robustness for previous methods and ours. D. Avg.: the average results on the destructive attacks. C. Avg.: the average results on the constructive attacks. R. Avg.: the average results on the reconstructive attacks. Avg.: the average results on all the attacks. B.: Bit Accuracy (%). T.: TPR@0.01FPR (%). S.Signa.: StableSignature. S.Stamp: StegaStamp. DT: DiffuseTrace. The numbers in parentheses are the bit lengths. **Mark** indicates that the metrics of our method are better than or equal to the ones of the previous methods. Underline indicates the best results of the previous methods.

Method	Untouched watermarked images						D. Avg.		C. Avg.		R. Avg.		Avg.	
	FID↓	SSIM↑	NIQE↓	PIQE↓	B.	T.	B.	T.	B.	T.	B.	T.	B.	T.
MS-COCO 2017 Evaluation Lin et al. [2014]														
TreeRing	26.38	0.02	13.05	11.95	-	97.40	-	48.30	-	43.77	-	38.20	-	44.67
S.Signa. (48)	25.75	0.92	<u>12.77</u>	10.98	99.45	<u>100.0</u>	58.65	25.71	68.19	49.36	59.83	34.82	60.91	33.17
LaWa (48)	<u>24.72</u>	0.93	<u>12.82</u>	<u>10.92</u>	<u>99.92</u>	<u>100.0</u>	84.07	74.55	87.28	88.94	81.96	82.57	84.08	79.83
RoSteALS (56)	35.60	0.93	15.81	44.35	96.69	94.69	<u>84.84</u>	<u>88.45</u>	<u>96.57</u>	<u>95.25</u>	85.10	74.07	87.26	85.50
S.Stamp (56)	25.37	<u>0.95</u>	16.91	11.33	96.98	94.69	83.86	78.11	96.54	95.21	<u>94.27</u>	<u>95.33</u>	<u>89.52</u>	<u>86.69</u>
DT (56)	31.86	0.00	15.39	18.74	58.03	16.42	54.05	8.14	56.60	13.05	56.51	12.21	55.30	10.34
Ours (48)	24.59	0.97	12.12	10.11	99.93	100.0	91.66	98.29	98.78	100.0	98.10	99.99	95.02	99.14
Ours (56)	24.53	0.95	12.33	9.86	<u>99.89</u>	100.0	92.41	96.70	98.94	100.0	98.20	100.0	95.45	98.35
Ours (64)	24.59	0.95	12.33	10.01	<u>99.95</u>	100.0	92.13	97.45	98.49	100.0	98.19	99.99	95.22	98.72
Ours (128)	24.59	0.96	12.16	10.14	<u>99.45</u>	100.0	85.94	96.38	<u>96.24</u>	<u>100.0</u>	<u>93.66</u>	<u>99.96</u>	90.32	98.18
Flickr30k Evaluation Young et al. [2014]														
TreeRing	37.03	0.02	13.48	10.42	-	89.10	-	49.26	-	40.59	-	42.74	-	45.57
S.Signa. (48)	36.89	0.93	13.15	10.52	99.69	<u>100.0</u>	58.62	25.51	68.84	50.10	59.99	36.51	61.07	33.73
LaWa (48)	<u>35.08</u>	0.93	<u>12.76</u>	<u>9.58</u>	<u>99.92</u>	<u>100.0</u>	81.30	68.56	82.79	80.91	76.75	75.49	80.23	73.11
RoSteALS (56)	42.01	0.93	16.31	44.98	96.49	94.60	<u>84.80</u>	<u>88.37</u>	92.90	88.22	93.37	<u>94.68</u>	88.99	<u>90.23</u>
S.Stamp (56)	36.70	<u>0.95</u>	17.49	11.01	96.96	94.66	84.45	79.68	<u>96.56</u>	<u>95.09</u>	<u>94.21</u>	94.63	<u>89.80</u>	87.25
DT (56)	44.14	0.01	15.47	18.60	57.82	16.11	53.83	8.10	55.34	11.17	56.13	12.09	54.82	9.91
Ours (48)	35.52	0.97	12.43	9.57	99.96	100.0	93.62	98.34	98.44	100.0	98.73	99.98	96.12	99.16
Ours (56)	35.92	0.96	12.66	9.19	99.92	100.0	93.78	97.00	98.48	100.0	98.85	100.0	96.24	98.50
Ours (64)	35.49	0.95	12.64	9.40	99.97	100.0	92.70	97.65	98.39	100.0	98.74	99.99	95.65	98.82
Ours (128)	35.30	0.97	12.44	9.52	<u>99.84</u>	100.0	86.54	96.40	<u>96.12</u>	100.0	94.94	100.0	90.98	98.20

4.1.2 Watermark Baselines

Six recently proposed watermarking methods are used as our baselines for comparison, i.e. StegaStamp Tancik et al. [2020], StableSignature Fernandez et al. [2023], RoSteALS Bui et al. [2023], LaWa Rezaei et al. [2024], TreeRing Wen et al. [2023], and DiffuseTrace Lei et al. [2024]. For StegaStamp, StableSignature, RoSteALS, and LaWa, the official codes and checkpoints are used to report the results. The lengths of message bits for the four methods are 56, 48, 56, and 48 respectively. For TreeRing, we follow the settings suggested by Wen et al. [2023] using the official codes, and inject the watermark with a ring radius of 10. For DiffuseTrace, we set the length of message bits as 56 bits and use the official codes and configurations to train the models.

4.1.3 LW Structure

For the message coupler, a U-net is used to fuse latent images and encoded messages. It has the same structure as the noise predictor ϵ_θ in Stable Diffusion except for the cross-attention modules. For the message decoupler, another U-net which has the same structure with the coupler is used to decouple encoded messages from latent images. The default methods are used to initialize the parameters of the decoupler. For the message encoder, four fully connected layers are used to map messages into the latent space. $Tanh(\cdot)$ is used as the activation function. For the message decoder, four fully connected layers are used to map decoupled latent images into the form of bits. And $Tanh(\cdot)$ is also used as the activation function. For outputs of the decoder, the values greater than 0 are assigned 1 and the values less than 0 are assigned 0.

4.1.4 LW Training

AdamW Loshchilov and Hutter [2018] is used to optimize the model. For the message encoder and decoder, the learning rate in Step 1 is set to $1e-4$ and in Step 3 is $1e-5$. For the message coupler and decoupler, the learning rate in Step 2 is set to $1e-3$ and in Step 3 is $1e-5$. τ_1 , τ_2 and τ_3 are set to 0.990, 0.045 and 0.900. α_1 , α_2 and α_3 are set to 1.5, 1.0 and 1.0 respectively. The batch size is 2. In Step 3, after the exponential moving average of Bit accuracy reaches 99.00%, we proceed to train the model for one more epoch and then terminate the training process. No data augmentation or noise layer is used during training. The latent diffusion model used in the experiments is Stable Diffusion v1.4. DDIM sampler Song et al. [2020] is used in the generation process and the sampling step is 50.

4.1.5 Attack Methods

The following 10 attacks are used for robustness evaluation in our experiments.

- Destructive attacks: Brightness distortion, contrast distortion, JPEG compression, Gaussian noising, and Cropping.
- Constructive attacks: Gaussian denoising and BM3D denoising Dabov et al. [2007].
- Reconstructive attacks Zhao et al. [2023b]: SD (v2.1) Rombach et al. [2022], VAE-Cheng Cheng et al. [2020] and VAE-BMSHJ Ballé et al. [2018].

The distortion factors of brightness and contrast are set to 0.1. The quality factor of JPEG is set to 0.1. The standard deviation of Gaussian Noising is set to 1.0. These options are significantly more challenging than existing studies Tancik et al. [2020], Bui et al. [2023], Wen et al. [2023], Fernandez et al. [2023], Zhao et al. [2023b]. For Cropping&Resizing, each image is cropped proportionally along its side and re-scaled to its original size. The proportion is set to 50%. When the proportion is above 50%, the performance of all the methods drops drastically and we cannot distinguish them effectively. Actually, excessive crops can seriously destroy images hence they do not often happen in daily use. For Gaussian Denoising, the kernel width is set to 9. For BM3D, the standard deviation of noise is set to 0.9. When the parameters of Gaussian Denoising and BM3D increase, the performance of the methods remains stable. For the reconstructive attacks, we use the parameters recommended by Zhao et al. [2023b].

4.1.6 Evaluation Metrics

For image quality, two reference-based metrics, i.e. Frchet Inception Distance (FID) and Structural Similarity Index Measure (SSIM), and two no-reference metrics, i.e. Natural Image Quality Evaluator score (NIQE) Mittal et al. [2013] and Perception-based Image Quality Evaluator score (PIQE) Venkatanath et al. [2015], are used. FID measures the distribution difference between 5,000 real images and 5,000 generated images. The real images are from COCO or Flickr30k and have the corresponding captions used for generation. SSIM measures the similarity between watermarked images and vanilla ones. NIQE and PIQE measure the perceptual quality of images based on the statistical properties of natural images and human vision systems respectively. Vanilla images refer to the generated images by the same prompts with the same diffusion model but without using watermarking methods. Image quality is evaluated on untouched watermarked images, which suffer no attack.

For watermark robustness, True Positive Rate at 0.01 False Positive Rate (TPR@0.01FPR) is used to quantify the performance of the identification task, and Bit Accuracy is used to quantify the performance of the attribution task. Following Fernandez et al. [2023] and Zhao et al. [2023b], we define TPR@0.01FPR as the identification accuracy using the thresholds when the theoretical FPR is less than 0.01, assuming that the matching or mismatching of each bit between injected and extracted messages can be treated as an i.i.d. variable and obeys the Bernoulli distribution with parameter 0.5. The thresholds for 48, 56, 64, and 128 bits are 33, 38, 42, and 78 bits respectively. Please refer to the supplementary material for more details about it. Bit Accuracy refers to the proportion of correctly extracted bits. We randomly generate binary messages for each bit length, and then they are fixed across the experiments as the ground-truth labels. For StableSignature, the official message is used, which has been fixed by the fine-tuned model.

We further evaluate the overall performance of image quality and watermark robustness. First, we unify the ranges and perform a positive transformation for FID, NIQE, and PIQE. We calculate the ratio of the metrics of vanilla images to the metrics of watermarked images. Then, we report the average of FID (unified and transformed), SSIM, NIQE (unified and transformed), and PIQE (unified and transformed), and the average of BitACC and TPR@0.01FPR under the three types of attacks. For TreeRing, only TPR@0.01FPR is averaged. The results have been reported in Fig.1.

Table 2: The detailed results on the attacks on MS-COCO 2017 captions. Mark indicates that the metrics of our method are better than or equal to the ones of the previous methods. Underline indicates the best results of the previous methods.

Method	D. Attack						C. Attack			R. Attack			
	Bright	Contrast	JPEG	Noising	Crop	Avg.	Gaussian	BM3D	Avg.	SD (v2.1)	VAE (Cheng)	VAE (BMSHJ)	Avg.
Bit Accuracy													
TreeRing	-	-	-	-	-	-	-	-	-	-	-	-	-
S.Signa. (48)	47.59	41.95	60.60	47.11	<u>95.99</u>	58.65	88.95	47.43	68.19	46.73	70.96	61.81	59.83
LaWa (48)	<u>99.79</u>	95.10	79.15	53.83	92.46	84.07	<u>99.40</u>	75.15	87.28	79.46	83.21	83.21	81.96
RoSteALS (56)	95.29	<u>95.58</u>	91.67	<u>73.23</u>	68.41	<u>84.84</u>	96.69	<u>96.45</u>	<u>96.57</u>	68.80	92.20	94.30	85.10
S.Stamp (56)	95.18	83.09	<u>91.97</u>	63.77	85.28	83.86	97.16	95.91	96.54	<u>89.20</u>	<u>96.80</u>	<u>96.80</u>	<u>94.27</u>
DT (56)	57.46	57.29	55.19	50.65	49.67	54.05	58.09	55.10	56.60	57.12	56.17	56.25	56.51
Ours (48)	98.21	<u>96.96</u>	92.81	79.16	91.18	<u>91.66</u>	99.90	97.66	98.78	99.09	97.27	97.93	98.10
Ours (56)	98.97	97.31	92.70	79.46	93.63	92.41	99.88	97.99	98.94	99.26	97.33	98.01	98.20
Ours (64)	98.69	<u>97.60</u>	92.63	78.30	93.43	92.13	99.93	97.05	98.49	99.19	97.44	97.95	98.19
Ours (128)	93.06	90.88	84.10	72.40	89.26	<u>85.94</u>	97.37	95.10	96.24	<u>95.13</u>	92.77	93.08	93.66
TPR@0.01FPR													
TreeRing	73.51	65.13	23.59	3.65	75.63	48.30	82.56	4.97	43.77	52.68	31.46	33.47	38.20
S.Signa. (48)	1.52	0.04	28.03	0.00	<u>98.96</u>	25.71	98.70	0.01	49.36	0.38	69.73	34.35	34.82
LaWa (48)	<u>100.0</u>	92.81	85.23	2.79	91.90	74.55	<u>100.0</u>	77.87	88.94	86.39	80.64	80.69	82.57
RoSteALS (56)	95.08	<u>95.18</u>	<u>94.67</u>	<u>85.23</u>	72.11	<u>88.45</u>	94.79	<u>95.70</u>	<u>95.25</u>	41.20	88.70	92.30	74.07
S.Stamp (56)	94.93	88.65	91.94	20.16	94.86	78.11	95.56	94.86	95.21	<u>95.64</u>	<u>95.61</u>	<u>94.73</u>	<u>95.33</u>
DT (56)	13.82	14.11	10.53	1.74	0.52	8.14	16.79	9.3	13.05	13.61	11.27	11.75	12.21
Ours (48)	99.98	<u>99.98</u>	99.94	93.28	98.26	98.29	100.0	100.0	100.0	100.0	99.96	100.0	99.99
Ours (56)	99.98	99.46	99.42	85.54	99.11	96.70	100.0	100.0	100.0	100.0	100.0	100.0	100.0
Ours (64)	100.0	100.0	99.98	87.36	99.92	97.45	100.0	100.0	100.0	100.0	99.96	100.0	99.99
Ours (128)	100.0	100.0	99.98	84.08	97.84	96.38	100.0	100.0	100.0	100.0	99.90	99.98	99.96

4.2 Main Results

In Tab.1, we report an overview of image quality and watermark robustness results. From the perspective of image quality, among the compared methods, LaWa excels over other methods in terms of FID and PIQE for both COCO and Flickr captions. It demonstrates that LaWa has an advantage in the perceptual quality of the watermarked images. StableSignature also presents an advantage in the perceptual quality of the watermarked images. StegaStamp achieves superior performance on SSIM but inferior performance on NIQE, indicating its poor perceptual quality. The poor PIQE of RoSteALS on two evaluation sets suggests a large gap between the perceptual quality of the watermarked images and the human vision systems. Besides, its poor FID further demonstrates the significant negative impact on image quality. For TreeRing and DiffuseTrace, their SSIMs are significantly inferior to others because editing the sampled noise changes the content of the generated images. Under the same number of message bits, LW exceeds or is equal to these existing methods on the four metrics in most cases, especially on FID, NIQE, and PIQE. It shows that compared with the previous methods, LW can watermark generated images with the smallest difference and the closest perceptual quality to vanilla ones. When the number of message bits is 64 or even 128, LW is still superior in image quality.

From the perspective of watermark robustness, it can be seen that StegaStamp and RoSteALS have stronger resistance to the attacks than other methods. The robustness of StegaStamp is stronger than RoSteALS for reconstructive attacks, and RoSteALS has an advantage in resisting destructive attacks. When we focus on our proposed LW, under the same (48, 56) or even more number (64) of message bits, the average results on the 10 attacks are all higher than StegaStamp and RoSteALS, at least 5% higher on Bit Accuracy and 11% higher on TPR@0.01FPR. When the number of bits is 128, a few BitACC is inferior to these two methods, but the margin is negligible, and its average robustness on all the attacks remains superior to them. The detailed results on each attack for COCO captions are shown in Tab.2, and the results for Flickr captions can be found in the supplementary material. Tab.2 demonstrates that our method has obvious advantages

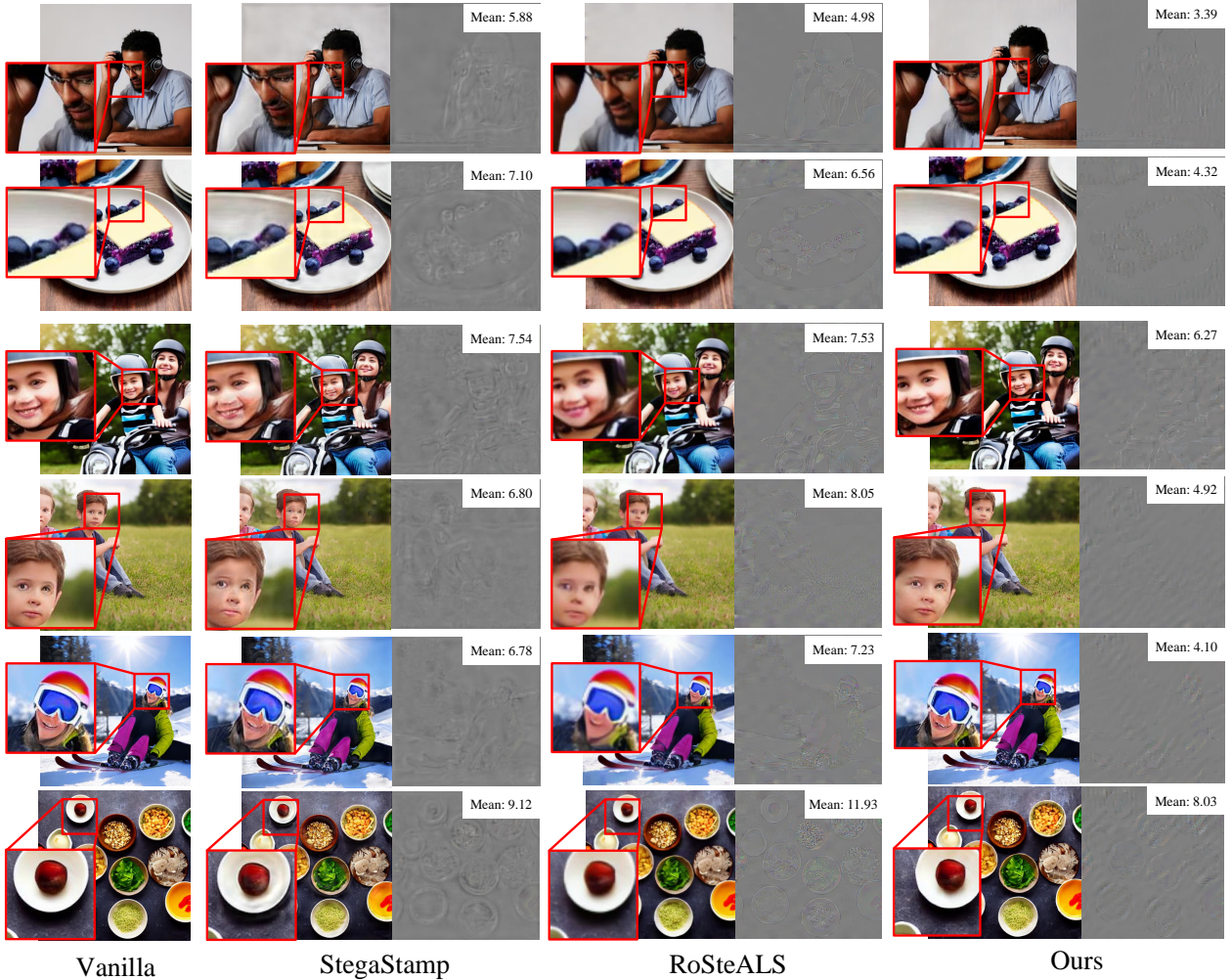


Figure 4: The clean images and the images watermarked by StegaStamp Tancik et al. [2020] (56 bits), RoSteALS Bui et al. [2023] (56 bits), and LW (56 bits). The residual images between the watermarked images and the clean images are given, with the mean absolute pixel difference in the upper right corner.

over the compared methods in resisting various attacks, except for Cropping. For Cropping, StableSignature achieves the best performance, while LW lags behind it by nearly 5% for the same number of bits. However, StableSignature exhibits significantly poor performance under other attacks. As the method closest to ours in image quality, LaWa exhibits poor watermark robustness, especially on the reconstructive attacks.

Finally, we give some examples of images watermarked by StegaStamp, RoSteALS, and ours in Fig.4. StegaStamp and RoSteALS exhibit better robustness compared with other methods. However, it can be seen that the images watermarked by StegaStamp have obvious shadows at the edges and bright areas, and the images watermarked by RoSteALS are blurry while our method does not have these problems. Fig.4 also shows the residuals and the mean absolute pixel difference between the vanilla and watermarked images, demonstrating LW’s image quality closer to the vanilla images. Please refer to the supplementary material for the images watermarked by our method with 48, 56, 64, and 128-bit messages. The examples, along with the radar chart shown in Fig.5, further illustrate the trade-off between image quality and watermark robustness in existing methods, and our proposed LW significantly reduces the contradiction between the two.

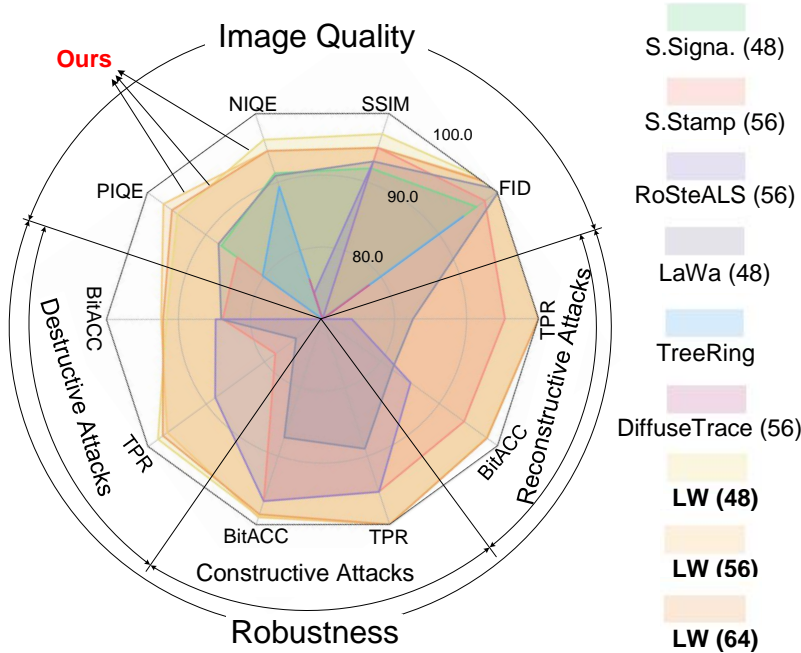


Figure 5: The radar chart for a comprehensive evaluation. The metrics are unified and transformed using the method mentioned in Sec.4.1.

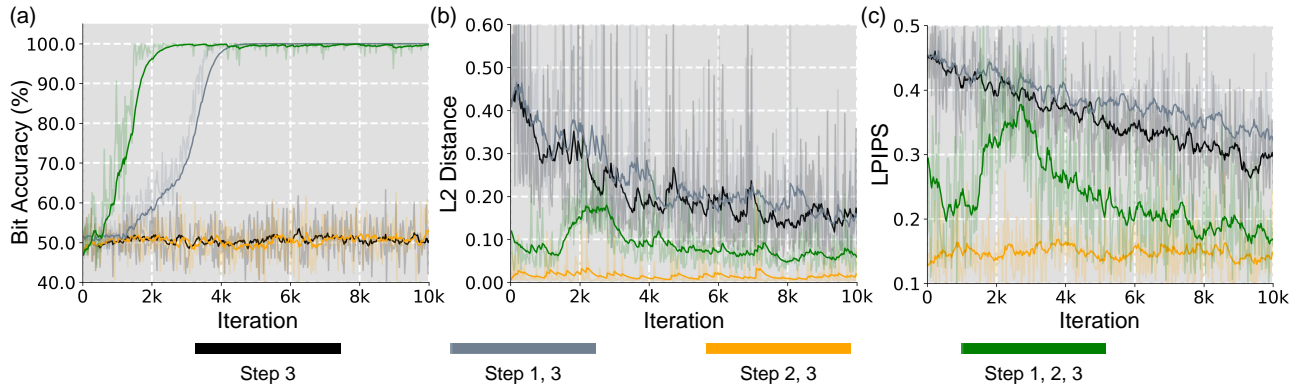


Figure 6: The training curves using one or more of the three steps of the progressive training strategy. (a) Bit Accuracy. (b) L2 distance of latent images (Eq.7). (c) Learned Perceptual Image Patch Similarity (LPIPS) loss Zhang et al. [2018] (Eq.8). Step 1 pre-trains the message encoder and decoder. Step 2 pre-trains the message coupler. Step 3 is the formal training.

4.3 Ablation Studies

4.3.1 Training Strategy

To verify the effectiveness of each step in the three-step progressive training strategy, we plot the training curves of Bit Accuracy, \mathcal{L}_z (Eq.7) and \mathcal{L}_I (Eq.8) using one or more of the training steps in Fig.6. From Fig.6 (a), we can see that the message encoder and decoder cannot be optimized without Step 1. Fig.6 (b) and (c) show that LW converges faster and the difference between watermarked and vanilla images is smaller with Step 2. The proposed training strategy can help LW obtain watermark injection and detection abilities while retaining image quality better.

Table 3: The results of using different latent channel(s) for watermark injection on MS-COCO 2017 captions. The differences between using Channel 0 and other channel(s) are given. **Mark** denotes the decreasing metrics.

Channel(s)	Untouched watermarked images					D. Avg. B.	C. Avg. B.	R. Avg. B.	Avg. B.
	FID ↓	SSIM ↑	NIQE ↓	PIQE ↓	B.				
0 (Used)	24.59	0.95	12.33	10.01	99.95	92.13	98.49	98.19	96.27
1	+0.13	+0.01	-0.21	-0.32	-0.46	-0.63	-0.97	-1.55	-0.97
2	+0.16	-0.07	+0.20	-0.66	-0.10	-0.51	-1.23	-2.63	-1.29
3	-0.34	-0.03	-0.21	-0.14	-0.04	-0.13	-0.37	-1.33	-0.54
0,1,2,3	+0.51	+0.01	-0.71	+0.58	-0.16	-0.31	-0.94	-2.00	-0.94

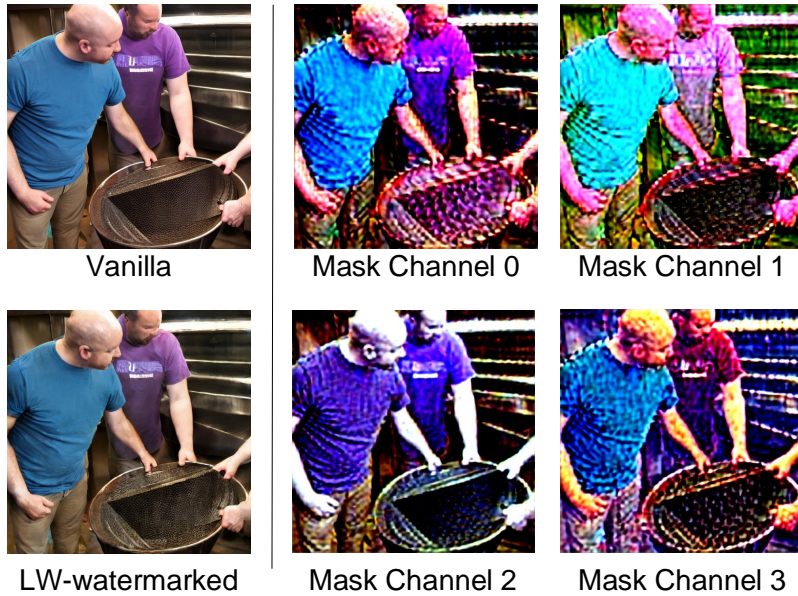


Figure 7: An example for visualizing the impact of each channel in the latent space on the generated images. On the left, it presents the vanilla-generated image alongside the LW-watermarked one. On the right, it presents the generated images with one latent channel masked. The channel is masked after the diffusion process but before the decoding.

4.3.2 Injection Channel

By coupling messages with various channels of latent images, we observe diverse effects on image quality and watermark robustness. In Eq.3, encoded messages are coupled with Channel 0 of latent images. We further evaluate other options and summarize the results in Tab.3. Our experiments indicate that selecting other channels or all channels for watermark injection often hurt its robustness while sometimes it can improve image quality. Considering all the metrics, we recommend selecting Channel 0 for injecting watermarks.

To delve into the reason why selecting different channels brings different performances, we conduct an ablation experiment on the generated images. Specifically, we mask each channel in the latent space respectively after the diffusion process but before the decoding, and then observe the changes in the generated images. Our finding is that masking one channel causes a change in the hues of images, and masking different channels causes different degrees of change, leading to different trade-offs between watermark robustness and image quality. An example is shown in Fig.7. In this example, when we mask Channel 1 and Channel 3, the background of the image appears to have distinct green and purple components. When we mask Channel 2, the blue T-shirt turns purple. When we mask Channel 0, overall, its hue is closer to the vanilla image. The above observation reveals that when watermarks with equal strength are injected into the latent space, selecting Channel 0 can ensure maximal consistency with the vanilla image. It explains why injecting watermarks into Channel 0 can achieve better image quality and watermark robustness at the same time. We speculate that the difference in the effects of the channels is formed spontaneously when training the autoencoder, which needs further study.

Table 4: The results of LW with the latent training strategy and the proposed progressive training strategy (64 bits).

Strategy	Untouched			Attacked
	FID↓	SSIM↑	BitACC↑	Avg. BitACC↑
Latent	43.02	0.83	99.56	88.83
Progressive	24.59	0.95	99.95	95.22

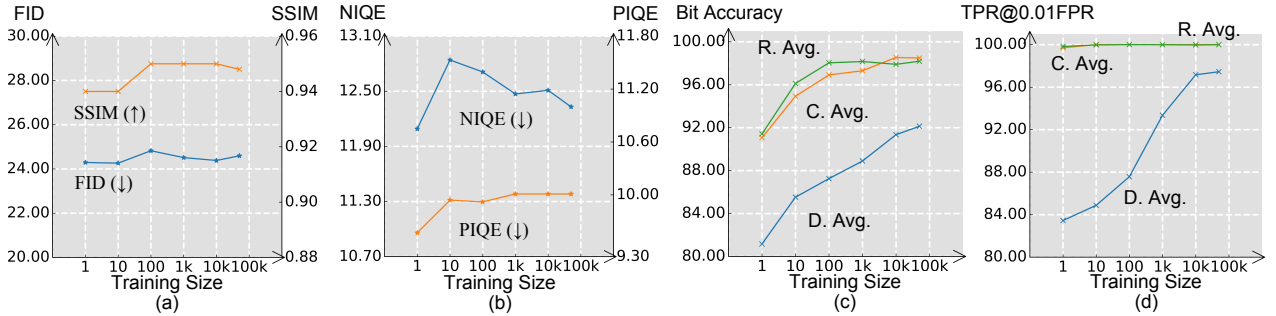


Figure 8: The change of performance with respect to the size of training data. (a) The reference-based metrics for image quality: FID and SSIM. (b) The no-reference metrics for image quality: NIQE and PIQE. (c) The metrics for watermark robustness: Bit Accuracy under the three attack categories. (d) The metrics for watermark robustness: TPR@0.01FPR under the three attack categories.

4.4 Additional Discussions

4.4.1 Necessity of The Progressive Training Strategy

In this paper, the progressive training strategy is proposed to address the difficulty in training the watermarking-related modules. As mentioned in Sec.1, it stems from the non-adaptation of the watermarking modules and the latent encoder/decoder in the training process. Since the watermark injection and detection are performed entirely in the latent space, we try the latent training strategy to avoid the presence of the latent encoder/decoder. The latent training strategy refers to training the modules entirely in the latent space. The latent images are fed into the message decoupler directly and not decoded into the pixel space during training. All the modules do not undergo any pre-training. The loss \mathcal{L}_I for the pixel images is also removed. The results are shown in Tab.4. It shows that the latent training strategy significantly degrades both image quality and watermark robustness. The underlying reason lies in the absence of the pixel space during the training process, which creates a gap between the training and inference phases. On the one hand, due to the lack of the visual perception loss, the embedded watermarks exert a more pronounced effect on image quality. On the other hand, the apparent deterioration in image quality renders the watermarks more vulnerable to attacks that target the images themselves. Therefore, it is necessary to introduce the decoder and encoder in the training, which justifies the necessity of the proposed training strategy.

4.4.2 Training Size

Fig.8 illustrates the performance of image quality and watermark robustness when training LW with varying training sizes of 1, 10, 100, 1k, 10k, and 50k images. Notably, the training size has a more significant influence on NIQE, BitACC, and TPR@0.01FPR compared to other metrics. They increase rapidly as the training size increases, while the rest of the metrics change slowly. When the size reaches 50k, the change in most metrics becomes relatively minor, leading us to select this size for training LW. It is worth mentioning that the size of the training data employed in this work is smaller than the 100k images used in RoSteALS Bui et al. [2023]. StegaStamp Tancik et al. [2020] and StableSignature Fernandez et al. [2023] do not provide specific details regarding the size of the training data from MIRFLICKR Huiskes and Lew [2008] and MS-COCO Lin et al. [2014] that they use respectively.

4.4.3 Results on Vanilla Images

We evaluate the False Positive Rate (FPR) of LW using the thresholds for TPR@0.01FPR. The evaluation is conducted on the vanilla images generated by the Stable Diffusion Model with the same prompts used in the evaluation on MS-COCO 2017 Lin et al. [2014] and Flickr30k Young et al. [2014]. The results are shown in Tab.5. We also report the

Table 5: The results of LW on the vanilla images. False Positive Rate (FPR, %) are reported with the corresponding theoretical values. The thresholds are the ones used to calculate TPR@0.01FPR in the experiments. The vanilla images are generated by the Stable Diffusion with the same prompts in the evaluation on MS-COCO 2017 Lin et al. [2014] and Flickr30k Young et al. [2014].

# of Bits	Theoretical	COCO	Flickr30k
48	0.0066	0.0074	0.0074
56	0.0052	0.0056	0.0056
64	0.0084	0.0080	0.0080
128	0.0083	0.0072	0.0078

Table 6: The inference time of the methods. The results are averaged over 5,000 images. The numbers in parentheses are the bit lengths. **Bold** results indicate the best ones and underline results indicate the second ones.

Method	Time (millisecond)		
	Injection	Extraction	Total
S.Signa. (48)	0.0	<u>43.2</u>	43.2
S.Stamp (56)	140.2	168.2	308.4
RoSteALS (56)	305.0	76.9	381.9
LaWa (48)	118.9	11.6	130.5
TreeRing	17.7	1176.3	1194.0
DiffuseTrace (56)	<u>2.2</u>	3926.8	3929.0
LW (56)	67.8	60.1	<u>127.9</u>

corresponding theoretical values under the thresholds. Tab.5 shows that the FPR of LW is very close to the theoretical values under various lengths of message bits and is lower than 0.01 as well. It demonstrates that the theoretical assumptions and calculation methods of TPR@0.01FPR are suitable for LW.

4.4.4 Time Efficiency

In addition to a low training cost and high performance, a good watermarking method should also have a low time cost for watermark injection and extraction. In this section, we measure the time efficiency of the methods. The results are averaged over 5,000 images with a size of 512×512 and reported in Tab.6. The inference time of LW ranks second, which is faster than most of the compared methods.

4.4.5 Limitation

LW lacks rotation invariance, which is a limitation of our method. While it retains robustness to minor image rotations, LW fails to effectively resist large rotations. To illustrate it, we conduct the experiments by rotating images at varying angles and comparing the extraction performance of various methods. Our findings reveal that for a rotation angle of 5° , LW (56 bits) achieves a BitACC exceeding 95%. However, as the angle surpasses 10° , the BitACC of LW (56 bits) drops below 60%, which outperforms RoSteALS and StegaStamp but trails behind StableSignature. Notably, large rotations can be easily detected and rectified, offering a potential pretext defense mechanism to mitigate the shortcomings of existing methods, including ours. We leave the exploration of watermarking methods in the latent diffusion space with rotation invariance as future work.

5 Conclusion

In this paper, we propose LW with a progressive training strategy to root watermarks in latent space for latent diffusion models, to identify and attribute generated images. Compared with previous methods, the fundamental difference is that watermarks are injected and detected in latent diffusion space rather than pixel space. It weakens the direct correlation between image quality and watermark robustness and alleviates their contradiction. We evaluate the image quality and robustness against 10 attacks of LW as well as six previous methods on two datasets, demonstrating that the proposed method brings stronger robustness and higher image quality at the same time. We provide an effective tool for distinguishing and attributing synthetic images in the AIGC era.

References

- Jonathan Ho, Ajay Jain, and Pieter Abbeel. Denoising diffusion probabilistic models. In *Proceedings of the Advances in Neural Information Processing Systems (NeurIPS)*, volume 33, pages 6840–6851, 2020.
- Jiaming Song, Chenlin Meng, and Stefano Ermon. Denoising diffusion implicit models. In *Proceedings of the International Conference on Learning Representations (ICLR)*, 2020.
- Alexander Quinn Nichol and Prafulla Dhariwal. Improved denoising diffusion probabilistic models. In *Proceedings of the International Conference on Machine Learning (ICML)*, pages 8162–8171, 2021.
- Luping Liu, Yi Ren, Zhijie Lin, and Zhou Zhao. Pseudo numerical methods for diffusion models on manifolds. In *Proceedings of the International Conference on Learning Representations (ICLR)*, 2022.
- Prafulla Dhariwal and Alexander Nichol. Diffusion models beat GANs on image synthesis. In *Proceedings of the Advances in Neural Information Processing Systems (NeurIPS)*, volume 34, pages 8780–8794, 2021.
- Alexander Quinn Nichol, Prafulla Dhariwal, Aditya Ramesh, Pranav Shyam, Pamela Mishkin, Bob McGrew, Ilya Sutskever, and Mark Chen. GLIDE: Towards photorealistic image generation and editing with text-guided diffusion models. In *Proceedings of the International Conference on Machine Learning (ICML)*, pages 16784–16804, 2022.
- Shuyang Gu, Dong Chen, Jianmin Bao, Fang Wen, Bo Zhang, Dongdong Chen, Lu Yuan, and Baining Guo. Vector quantized diffusion model for text-to-image synthesis. In *Proceedings of the IEEE/CVF Conference on Computer Vision and Pattern Recognition (CVPR)*, pages 10696–10706, 2022.
- Robin Rombach, Andreas Blattmann, Dominik Lorenz, Patrick Esser, and Björn Ommer. High-resolution image synthesis with latent diffusion models. In *Proceedings of the IEEE/CVF Conference on Computer Vision and Pattern Recognition (CVPR)*, pages 10684–10695, 2022.
- Edward J Hu, Phillip Wallis, Zeyuan Allen-Zhu, Yuanzhi Li, Shean Wang, Lu Wang, Weizhu Chen, et al. LoRA: Low-rank adaptation of large language models. In *Proceedings of the International Conference on Learning Representations (ICLR)*, 2021.
- Nataniel Ruiz, Yuanzhen Li, Varun Jampani, Yael Pritch, Michael Rubinstein, and Kfir Aberman. DreamBooth: Fine tuning text-to-image diffusion models for subject-driven generation. In *Proceedings of the IEEE/CVF Conference on Computer Vision and Pattern Recognition (CVPR)*, pages 22500–22510, 2023.
- Enze Xie, Lewei Yao, Han Shi, Zhili Liu, Daquan Zhou, Zhaoqiang Liu, Jiawei Li, and Zhenguo Li. DiffFit: Unlocking transferability of large diffusion models via simple parameter-efficient fine-tuning. In *Proceedings of the IEEE/CVF International Conference on Computer Vision (ICCV)*, pages 4230–4239, 2023.
- Clark Barrett, Brad Boyd, Elie Bursztein, Nicholas Carlini, Brad Chen, Jihye Choi, Amrita Roy Chowdhury, Mihai Christodorescu, Anupam Datta, Soheil Feizi, et al. Identifying and mitigating the security risks of generative AI. *Foundations and Trends in Privacy and Security (FTPS)*, 6(1):1–52, 2023.
- Sheng-Yu Wang, Oliver Wang, Richard Zhang, Andrew Owens, and Alexei A Efros. CNN-generated images are surprisingly easy to spot... for now. In *Proceedings of the IEEE/CVF Conference on Computer Vision and Pattern Recognition (CVPR)*, pages 8695–8704, 2020.
- Yuyang Qian, Guojun Yin, Lu Sheng, Zixuan Chen, and Jing Shao. Thinking in frequency: Face forgery detection by mining frequency-aware clues. In *Proceedings of the European Conference on Computer Vision (ECCV)*, pages 86–103, 2020.
- Ke Sun, Hong Liu, Taiping Yao, Xiaoshuai Sun, Shen Chen, Shouhong Ding, and Rongrong Ji. An information theoretic approach for attention-driven face forgery detection. In *Proceedings of the European Conference on Computer Vision (ECCV)*, pages 111–127, 2022.
- Zhendong Wang, Jianmin Bao, Wengang Zhou, Weilun Wang, Hezhen Hu, Hong Chen, and Houqiang Li. DIRE for diffusion-generated image detection. In *Proceedings of the IEEE/CVF International Conference on Computer Vision (ICCV)*, pages 22445–22455, 2023a.
- Lucy Chai, David Bau, Ser-Nam Lim, and Phillip Isola. What makes fake images detectable? Understanding properties that generalize. In *Proceedings of the European Conference on Computer Vision (ECCV)*, pages 103–120, 2020.
- Riccardo Corvi, Davide Cozzolino, Giada Zingarini, Giovanni Poggi, Koki Nagano, and Luisa Verdoliva. On the detection of synthetic images generated by diffusion models. In *Proceedings of the IEEE International Conference on Acoustics, Speech and Signal Processing (ICASSP)*, pages 1–5, 2023.
- Peter Lorenz, Ricard L. Durall, and Janis Keuper. Detecting images generated by deep diffusion models using their local intrinsic dimensionality. In *Proceedings of the IEEE/CVF International Conference on Computer Vision Workshops (ICCVW)*, pages 448–459, 2023.

- Jonas Ricker, Simon Damm, Thorsten Holz, and Asja Fischer. Towards the detection of diffusion model deepfakes. In *Proceedings of the International Conference on Learning Representations (ICLR)*, 2023.
- Ashif Raja. Active and passive detection of image forgery: A review analysis. *International Journal of Engineering Research and Technology (IJERT)*, 9(5):418–424, 2021.
- Xiaoshuai Wu, Xin Liao, and Bo Ou. SepMark: Deep separable watermarking for unified source tracing and deepfake detection. In *Proceedings of the 31st ACM International Conference on Multimedia (MM)*, page 1190–1201, 2023.
- Pierre Fernandez, Alexandre Sablayrolles, Teddy Furon, Hervé Jégou, and Matthijs Douze. Watermarking images in self-supervised latent spaces. In *Proceedings of the IEEE International Conference on Acoustics, Speech and Signal Processing (ICASSP)*, pages 3054–3058, 2022.
- Matthew Tancik, Ben Mildenhall, and Ren Ng. Stegastamp: Invisible hyperlinks in physical photographs. In *Proceedings of the IEEE/CVF Conference on Computer Vision and Pattern Recognition (CVPR)*, pages 2117–2126, 2020.
- Cheng Xiong, Chuan Qin, Guorui Feng, and Xinpeng Zhang. Flexible and secure watermarking for latent diffusion model. In *Proceedings of the 31st ACM International Conference on Multimedia (MM)*, pages 1668–1676, 2023.
- Quang Nguyen, Truong Vu, Cuong Pham, Anh Tran, and Khoi Nguyen. Stable Messenger: Steganography for message-concealed image generation. *arXiv preprint arXiv:2312.01284*, 2023.
- Tu Bui, Shruti Agarwal, Ning Yu, and John Collomosse. RoSteALS: Robust steganography using autoencoder latent space. In *Proceedings of the IEEE/CVF Conference on Computer Vision and Pattern Recognition (CVPR)*, pages 933–942, 2023.
- Zhenting Wang, Chen Chen, Yuchen Liu, Lingjuan Lyu, Dimitris Metaxas, and Shiqing Ma. How to detect unauthorized data usages in text-to-image diffusion models. *arXiv preprint arXiv:2307.03108*, 2023b.
- Pierre Fernandez, Guillaume Couairon, Hervé Jégou, Matthijs Douze, and Teddy Furon. The stable signature: Rooting watermarks in latent diffusion models. In *Proceedings of the IEEE/CVF International Conference on Computer Vision (ICCV)*, pages 22466–22477, 2023.
- Yunqing Zhao, Tianyu Pang, Chao Du, Xiao Yang, Ngai-Man Cheung, and Min Lin. A recipe for watermarking diffusion models. *arXiv preprint arXiv:2303.10137*, 2023a.
- Yuxin Wen, John Kirchenbauer, Jonas Geiping, and Tom Goldstein. Tree-Ring watermarks: Fingerprints for diffusion images that are invisible and robust. In *Proceedings of the Advances in Neural Information Processing Systems (NeurIPS)*, 2023.
- Xuandong Zhao, Kexun Zhang, Yu-Xiang Wang, and Lei Li. Generative autoencoders as watermark attackers: Analyses of vulnerabilities and threats. In *Proceedings of the International Conference on Machine Learning Workshop (ICMLW)*, 2023b.
- Tsung-Yi Lin, Michael Maire, Serge Belongie, James Hays, Pietro Perona, Deva Ramanan, Piotr Dollár, and C Lawrence Zitnick. Microsoft COCO: Common objects in context. In *Proceedings of the European Conference on Computer Vision (ECCV)*, pages 740–755, 2014.
- Xin Wang, Yudong Chen, and Wenwu Zhu. A survey on curriculum learning. *IEEE Transactions on Pattern Analysis and Machine Intelligence (TPAMI)*, 44(9):4555–4576, 2021.
- Richard Zhang, Phillip Isola, Alexei A Efros, Eli Shechtman, and Oliver Wang. The unreasonable effectiveness of deep features as a perceptual metric. In *Proceedings of the IEEE Conference on Computer Vision and Pattern Recognition (CVPR)*, pages 586–595, 2018.
- Jari Korhonen and Junyong You. Peak signal-to-noise ratio revisited: Is simple beautiful? In *Proceedings of the Fourth International Workshop on Quality of Multimedia Experience (QoMEX)*, pages 37–38, 2012.
- Zhou Wang, Alan C Bovik, Hamid R Sheikh, and Eero P Simoncelli. Image quality assessment: From error visibility to structural similarity. *IEEE Transactions on Image Processing (TIP)*, 13(4):600–612, 2004.
- Christoph Schuhmann, Romain Beaumont, Richard Vencu, Cade Gordon, Ross Wightman, Mehdi Cherti, Theo Coombes, Aarush Katta, Clayton Mullis, Mitchell Wortsman, et al. Laion-5b: An open large-scale dataset for training next generation image-text models. In *Proceedings of the Advances in Neural Information Processing Systems (NeurIPS)*, volume 35, pages 25278–25294, 2022.
- Jia Deng, Wei Dong, Richard Socher, Li-Jia Li, Kai Li, and Li Fei-Fei. ImageNet: A large-scale hierarchical image database. In *Proceedings of the IEEE/CVF Conference on Computer Vision and Pattern Recognition (CVPR)*, pages 248–255, 2009.
- Olaf Ronneberger, Philipp Fischer, and Thomas Brox. U-net: Convolutional networks for biomedical image segmentation. In *Proceedings of the 18th Medical Image Computing and Computer-Assisted Intervention (MICCAI)*, pages 234–241, 2015.

- Ilya Loshchilov and Frank Hutter. Decoupled weight decay regularization. In *Proceedings of the International Conference on Learning Representations (ICLR)*, 2018.
- Ingemar J. Cox, Matthew J. Miller, Jeffrey A. Bloom, Jessica Fridrich, and Ton Kalker. Digital watermarking and steganography. *Morgan Kaufmann*, 2007.
- Kevin Alex Zhang, Lei Xu, Alfredo Cuesta-Infante, and Kalyan Veeramachaneni. Robust invisible video watermarking with attention. *arXiv preprint arXiv:1909.01285*, 2019.
- Johannes Ballé, David Minnen, Saurabh Singh, Sung Jin Hwang, and Nick Johnston. Variational image compression with a scale hyperprior. In *Proceedings of the International Conference on Learning Representations (ICLR)*, 2018.
- Zhengxue Cheng, Heming Sun, Masaru Takeuchi, and Jiro Katto. Learned image compression with discretized gaussian mixture likelihoods and attention modules. In *Proceedings of the IEEE/CVF Conference on Computer Vision and Pattern Recognition (CVPR)*, pages 7939–7948, 2020.
- Yixiong Chen. X-iqe: explainable image quality evaluation for text-to-image generation with visual large language models. *arXiv preprint arXiv:2305.10843*, 2023.
- Ning Yu, Vladislav Skripniuk, Sahar Abdelnabi, and Mario Fritz. Artificial fingerprinting for generative models: Rooting deepfake attribution in training data. In *Proceedings of the IEEE/CVF International Conference on Computer Vision (ICCV)*, pages 14448–14457, 2021.
- Alexandre Lacoste, Alexandra Luccioni, Victor Schmidt, and Thomas Dandres. Quantifying the carbon emissions of machine learning. In *Proceedings of the Advances in Neural Information Processing Systems Workshop (NeurIPSW)*, 2019.
- Anish Mittal, Rajiv Soundararajan, and Alan C. Bovik. Making a "completely blind" image quality analyzer. *IEEE Signal Processing Letters*, 20(3):209–212, 2013.
- Jascha Sohl-Dickstein, Eric Weiss, Niru Maheswaranathan, and Surya Ganguli. Deep unsupervised learning using nonequilibrium thermodynamics. In *Proceedings of the International Conference on Machine Learning (ICML)*, pages 2256–2265, 2015.
- Kostadin Dabov, Alessandro Foi, Vladimir Katkovnik, and Karen Egiazarian. Image denoising by sparse 3-d transform-domain collaborative filtering. *IEEE Transactions on Image Processing (TIP)*, 16(8):2080–2095, 2007.
- Peter Young, Alice Lai, Micah Hodosh, and Julia Hockenmaier. From image descriptions to visual denotations: New similarity metrics for semantic inference over event descriptions. *Transactions of the Association for Computational Linguistics (ACL)*, 2:67–78, 2014.
- N Venkatanath, D Praneeth, Maruthi Chandrasekhar Bh, Sumohana S Channappayya, and Swarup S Medasani. Blind image quality evaluation using perception based features. In *IEEE National Conference on Communications (NCC)*, pages 1–6, 2015.
- Mark J Huiskes and Michael S Lew. The mir flickr retrieval evaluation. In *Proceedings of the 1st ACM International Conference on Multimedia Information Retrieval (ICMIR)*, pages 39–43, 2008.
- Yiyi Li, Xin Liao, and Xiaoshuai Wu. Screen-shooting resistant watermarking with grayscale deviation simulation. *IEEE Transactions on Multimedia (TMM)*, 2024.
- Wenguang He, Zhanchuan Cai, and Yaomin Wang. High-fidelity reversible image watermarking based on effective prediction error-pairs modification. *IEEE Transactions on Multimedia (TMM)*, 23:52–63, 2020.
- Chuan Qin, Xiaomeng Li, Zhenyi Zhang, Fengyong Li, Xinpeng Zhang, and Guorui Feng. Print-camera resistant image watermarking with deep noise simulation and constrained learning. *IEEE Transactions on Multimedia (TMM)*, 26: 2164–2177, 2024.
- Xin Zhong, Pei-Chi Huang, Spyridon Mastorakis, and Frank Y Shih. An automated and robust image watermarking scheme based on deep neural networks. *IEEE Transactions on Multimedia (TMM)*, 23:1951–1961, 2020.
- Han Fang, Zhaoyang Jia, Yupeng Qiu, Jiyi Zhang, Weiming Zhang, and Ee-Chien Chang. De-end: decoder-driven watermarking network. *IEEE Transactions on Multimedia (TMM)*, 25:7571–7581, 2022.
- Ahmad Rezaei, Mohammad Akbari, Saeed Ranjbar Alvar, Arezou Fatemi, and Yong Zhang. Lawa: Using latent space for in-generation image watermarking. *arXiv preprint arXiv:2408.05868*, 2024.
- Liangqi Lei, Keke Gai, Jing Yu, and Liehuang Zhu. Diffusetrace: A transparent and flexible watermarking scheme for latent diffusion model. *arXiv preprint arXiv:2405.02696*, 2024.

Appendix A Detailed Results on Flickr30k

The results on Flickr30k captions under the single-attack scenarios are shown in Tab.S1.

Table S1: The detailed results on the attacks on Flickr30k captions. D. Attack: the destructive attacks. C. Attack: the constructive attacks. R. Attack: the reconstructive attacks. S.Signa.: StableSignature. S.Stamp: StegaStamp. The numbers in parentheses are the numbers of encoded bits. Mark indicates that the B. and T. of our method are better than or equal to the ones of the previous methods. Underline indicates the best results of the previous methods.

Method	Bright		D. Attack				C. Attack			R. Attack			
	Bright	Contrast	JPEG	Noising	Crop	Avg.	Gaussian	BM3D	Avg.	SD (v2.1)	VAE (Cheng)	VAE (BMSHJ)	Avg.
Bit Accuracy													
TreeRing	-	-	-	-	-	-	-	-	-	-	-	-	-
S.Signa. (48)	46.71	41.66	60.66	47.10	<u>96.97</u>	58.62	89.74	47.94	68.84	45.72	71.44	62.80	59.99
LaWa (48)	92.62	91.60	76.73	53.49	92.07	81.30	92.07	73.51	82.79	71.77	81.48	77.00	76.75
RoSteALS (56)	94.98	<u>95.24</u>	91.61	<u>73.85</u>	68.33	<u>84.80</u>	96.49	89.30	92.90	<u>90.32</u>	94.77	95.03	93.37
S.Stamp (56)	<u>95.37</u>	83.69	<u>93.74</u>	64.40	85.04	84.45	<u>97.17</u>	<u>95.95</u>	<u>96.56</u>	88.91	<u>96.83</u>	<u>96.89</u>	<u>94.21</u>
DT (56)	56.65	56.45	55.08	50.71	50.26	53.83	56.42	54.25	55.34	56.57	56.02	55.80	56.13
Ours (48)	99.71	97.73	94.09	80.31	96.26	93.62	99.94	96.93	98.44	99.22	98.31	98.67	98.73
Ours (56)	99.01	98.49	94.96	79.69	96.73	93.78	99.44	97.51	98.48	99.14	98.74	98.68	98.85
Ours (64)	99.06	98.16	93.83	78.13	94.34	92.70	99.95	96.83	98.39	99.32	98.30	98.60	98.74
Ours (128)	93.92	91.81	84.68	72.26	90.03	86.54	97.60	94.63	96.12	95.76	94.46	94.61	94.94
TPR@0.01FPR													
TreeRing	71.92	68.93	27.97	2.95	74.51	49.26	77.73	3.44	40.59	56.51	34.50	37.22	42.74
S.Signa. (48)	1.20	0.06	26.86	0.00	<u>99.42</u>	25.51	<u>99.30</u>	0.90	50.10	0.12	71.98	37.44	36.51
LaWa (48)	85.56	84.77	78.13	2.70	91.63	68.56	85.59	76.23	80.91	66.53	79.30	80.63	75.49
RoSteALS (56)	94.88	<u>94.94</u>	94.44	<u>86.67</u>	70.90	<u>88.37</u>	94.64	81.80	88.22	<u>94.54</u>	<u>94.78</u>	94.72	<u>94.68</u>
S.Stamp (56)	<u>94.91</u>	88.60	<u>96.51</u>	23.13	95.23	79.68	95.34	<u>94.83</u>	<u>95.09</u>	94.40	94.72	<u>94.78</u>	94.63
DT (56)	14.97	13.51	9.60	1.53	0.89	8.10	12.67	9.66	11.17	13.63	11.14	11.49	12.09
Ours (48)	100.0	100.0	99.94	93.31	98.44	98.34	100.0	100.0	100.0	100.0	99.96	99.98	99.98
Ours (56)	100.0	100.0	100.0	85.69	99.32	97.00	100.0	100.0	100.0	100.0	100.0	100.0	100.0
Ours (64)	100.0	100.0	100.0	88.31	99.94	97.65	100.0	100.0	100.0	100.0	99.98	99.98	99.99
Ours (128)	100.0	100.0	99.96	83.93	98.12	96.40	100.0	100.0	100.0	100.0	100.0	100.0	100.0

Appendix B Examples of LW-Watermarked Images

The examples of images watermarked by LW are shown in Fig.S1 (48 bits), Fig.S2 (56 bits), Fig.S3 (64 bits) and Fig.S4 (128 bits).



Figure S1: The examples of images watermarked by LW (48 bits). The top of each set is the vanilla image generated by Stable Diffusion, and the bottom is the image watermarked by LW.

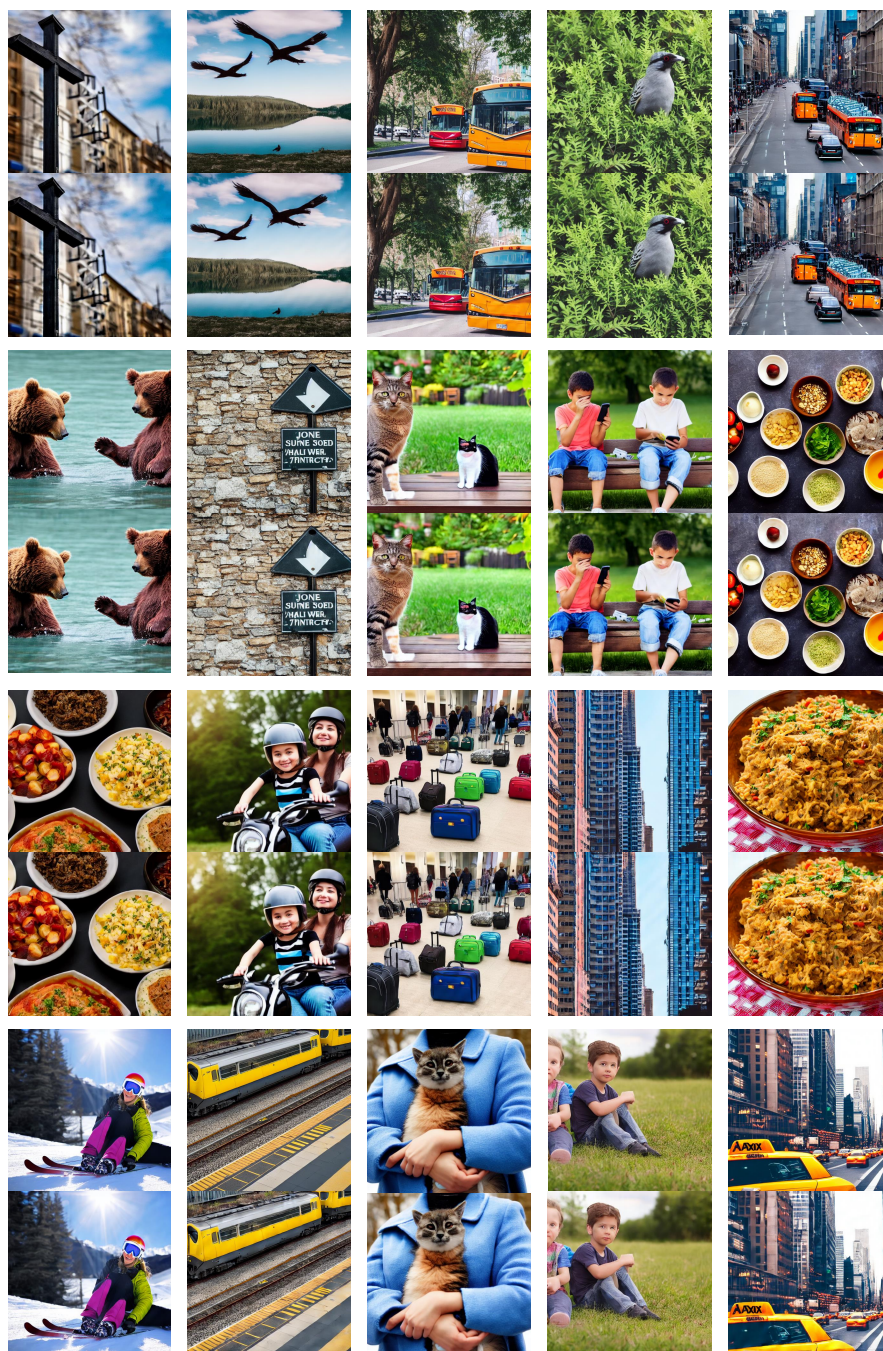


Figure S2: The examples of images watermarked by LW (56 bits). The top of each set is the vanilla image generated by Stable Diffusion, and the bottom is the image watermarked by LW.

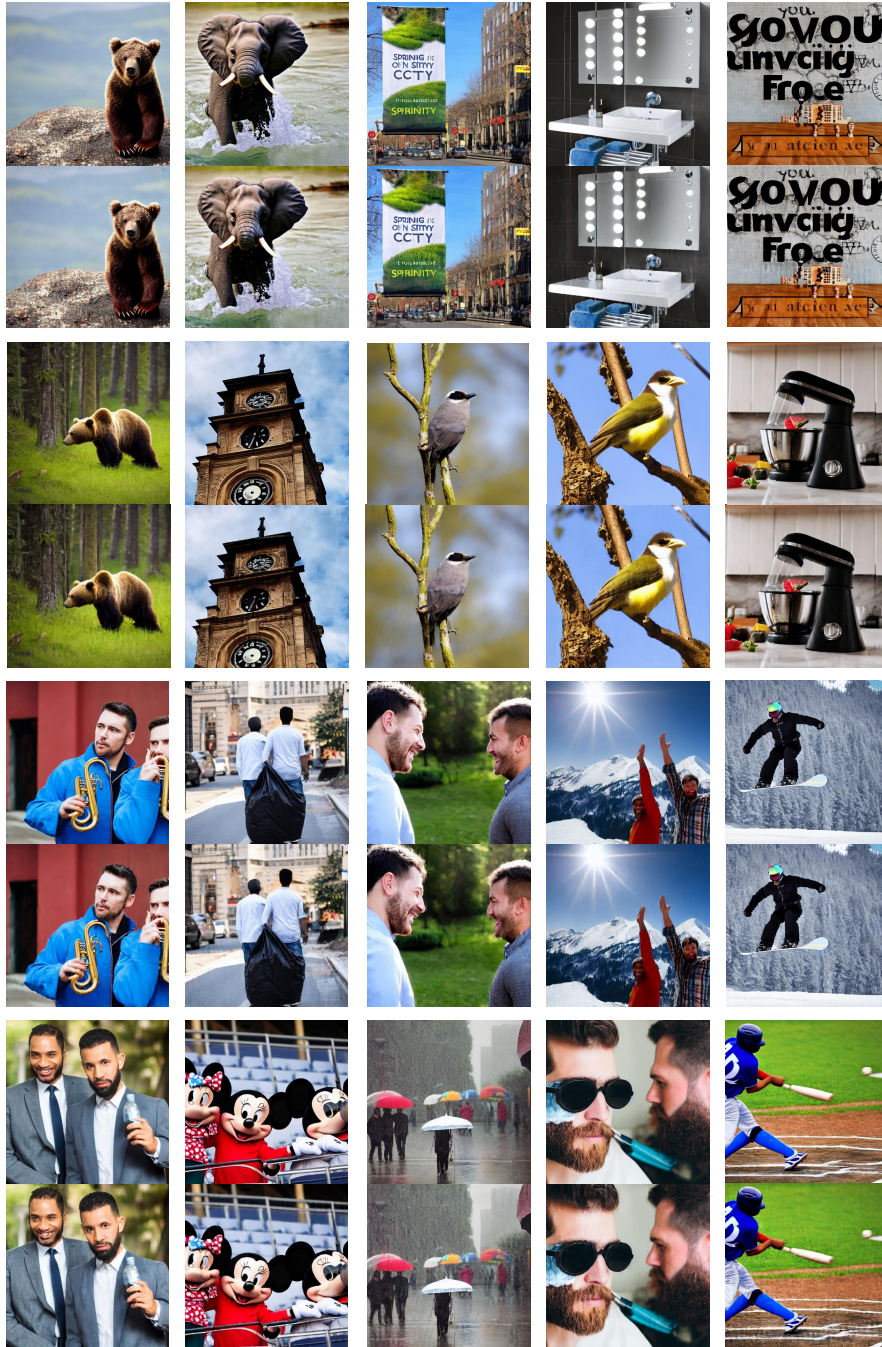


Figure S3: The examples of images watermarked by LW (64 bits). The top of each set is the vanilla image generated by Stable Diffusion, and the bottom is the image watermarked by LW.

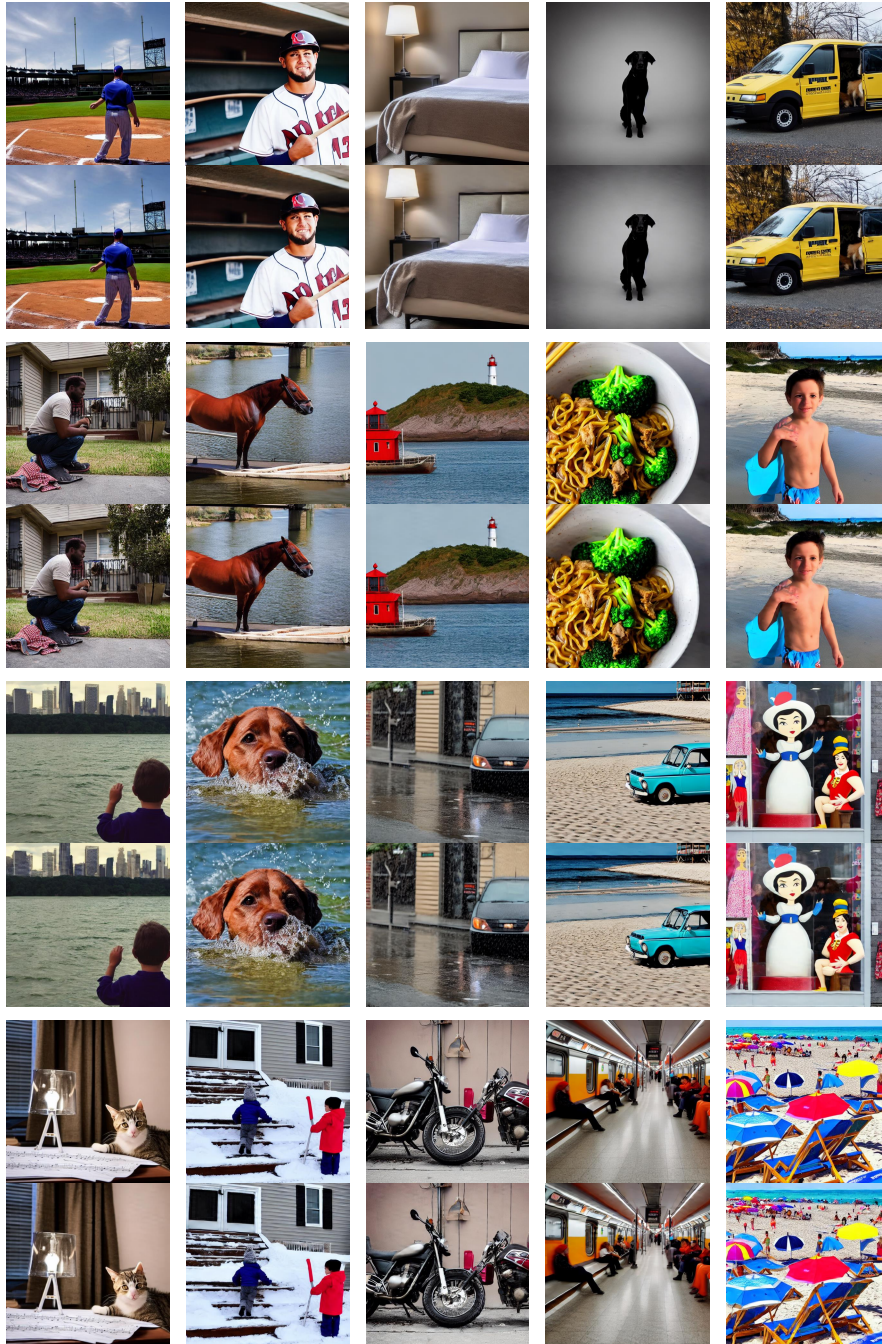


Figure S4: The examples of images watermarked by LW (128 bits). The top of each set is the vanilla image generated by Stable Diffusion, and the bottom is the image watermarked by LW.